

# Effects of Trehalose on Lipid Membranes under Rapid Cooling using All-Atom and Coarse-Grained Molecular Simulations

Published as part of *The Journal of Physical Chemistry* virtual special issue “Carol K. Hall Festschrift”.

Daniel J. Kozuch, Frank H. Stillinger, and Pablo G. Debenedetti\*



Cite This: *J. Phys. Chem. B* 2021, 125, 5346–5357



Read Online

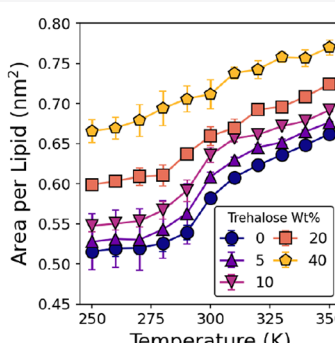
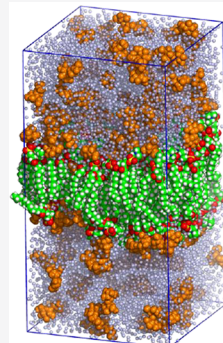
ACCESS |

Metrics & More

Article Recommendations

Supporting Information

**ABSTRACT:** We investigate the effect of the cryopreservative  $\alpha$ - $\alpha$ -trehalose on a model 1,2-dimyristoyl-*sn*-glycero-3-phosphocholine (DMPC) lipid membrane undergoing cooling from 350 to 250 K using all-atom (AA) and coarse-grained (CG) molecular dynamics simulation. In the AA simulations, we find that the addition of trehalose alters the  $L_\alpha$  (liquid crystalline) to  $P_\beta$  (ripple) phase transition, suppressing the major domain of the  $P_\beta$  phase and increasing the degree of leaflet interdigitation (the minor domain) which yields a thinner membrane with a higher area per lipid. Calculation of dihedral angle distributions for the lipid tails shows a greater fraction of *gauche* angles in the  $P_\beta$  phase as trehalose concentration is increased, indicating that trehalose increases lipid disorder in the membrane. In contrast, the CG simulations transition directly from the  $L_\alpha$  to the  $L_\beta$  (gel) phase upon cooling without exhibiting the  $P_\beta$  phase (likely due to increased lipid mobility in the CG system). Even so, the CG simulations show that the addition of trehalose clearly suppresses the  $L_\alpha$  to  $L_\beta$  phase transition, demonstrating that trehalose increases lipid disorder at low temperatures for the CG system, similar to the AA. Analysis using a two-state binding model provides net affinity coefficients between trehalose and the membrane as well as trehalose partition coefficients between the membrane interface and the bulk solution for both the AA and CG systems.



## INTRODUCTION

The influence of sugars on membranes has been of scientific interest for some time.<sup>1–4</sup> The nonreducing disaccharide  $\alpha$ - $\alpha$ -trehalose in particular has received attention for its remarkable properties as a cryopreservative agent (CPA).<sup>5–9</sup> As such, much effort has been expended in studying membrane-trehalose interactions at the atomistic level via molecular simulation, mainly under physiological conditions.<sup>10–17</sup> While some investigations have probed the effects of trehalose on membranes under dehydration and mechanical stress,<sup>18,19</sup> little work has yet been done to explore the effect of trehalose on membranes at low temperatures. Specifically, we are interested in the effects of trehalose on membranes under rapid cooling, similar to implementing cryopreservation through vitrification.<sup>20</sup>

An important aspect of membranes at low temperatures is the  $L_\alpha$  (liquid crystalline)-to- $L_\beta$  (gel) phase transition, wherein the membrane shifts from a more fluid state with relatively fast translational diffusion at high temperatures, to an arrested gel-like state at lower temperatures. This transition is particularly important as associated changes in the permeability and mechanical properties of the membrane are strongly implicated in the viability of cryopreserved specimens.<sup>21,22</sup> Evidence from differential scanning calorimetry (DSC) indicates that the

addition of trehalose to hydrated membranes decreases the temperature,  $T_m$ , of this transition and broadens the associated peak in the thermogram,<sup>23,24</sup> suggesting that one of the mechanisms through which trehalose provides cryoprotection is suppression of the fluid-to-gel transition.

To study the effects of trehalose on this transition and other membrane properties, we performed molecular dynamics simulations using all-atom (AA) and coarse-grained (CG) simulations under stepwise cooling from 350 to 250 K. The simulation system consists of a model lipid bilayer in contact with a solvent containing trehalose. The bilayer is composed of 1,2-dimyristoyl-*sn*-glycero-3-phosphocholine (DMPC) lipids, chosen for comparison to previously published results investigating the interaction between DMPC and trehalose.<sup>15,16,25</sup> DMPC, like other phosphatidylcholines, forms a pretransition ripple phase ( $P_\beta$ ) that appears between the  $L_\alpha$

Received: March 22, 2021

Revised: May 1, 2021

Published: May 12, 2021



and  $L_\beta$  phases.<sup>26–28</sup> The  $P_\beta$  phase is characterized by a sawtooth pattern composed of a thicker major domain and a thinner minor domain connected by a kink region.<sup>29,30</sup> Under our cooling procedure, we find that the AA simulations become trapped in this  $P_\beta$  phase, never fully transitioning to the  $L_\beta$  phase (which is observed below 275 K<sup>28</sup>). However, the CG simulations are observed to transition directly from the  $L_\alpha$  to the  $L_\beta$  phase. These transitions to more ordered phases under cooling ( $L_\alpha$  to  $P_\beta$  and  $L_\alpha$  to  $L_\beta$ ) are studied under a series of trehalose concentrations ranging from 0 to 40 wt %. Details of the molecular simulation are given in the “Methods” section, and results are given in the “Results and Discussion” section.

## METHODS

**AA Molecular Dynamics.** AA systems were prepared by first assembling a DMPC lipid bilayer with 5 nm of water on either side using the CHARMM Graphical User Interface (CHARMM-GUI).<sup>31–33</sup> The membrane and water (TIP3P) were both described by the CHARMM36m force field.<sup>34,35</sup> Five different trehalose concentrations (0, 5, 10, 20, and 40 wt % of the solvent) were then produced by inserting  $\alpha$ - $\alpha$ -trehalose molecules into the water layers on either side of the membrane and deleting overlapping water molecules. The resulting system contains from 9000 to 13 000 water molecules. See the Supporting Information for a list of all systems studied. Trehalose was described by a modified version<sup>36</sup> of the GLYCAM06<sup>37</sup> force field which corrects for overly attractive trehalose-trehalose interactions. We note that TIP3P is not an ideal water model for low temperatures, but given that it and other three-site water models are used to parametrize most commonly used biomolecule related force fields (including CHARMM36m and GLYCAM06), it was used for the body of this work. See the Supporting Information for further discussion and tests using different force fields.

Molecular dynamics simulations were performed using GROMACS 2020.2.<sup>38–41</sup> All systems were first energy-minimized using steepest descent and then equilibrated. Equilibration (as suggested by the CHARMM-GUI output) consisted of progressively raising the time step from 1 to 2 fs, while the membrane restraints were progressively turned off. See the Supporting Information for details. The last equilibration step was performed for a short period of 500 ps at 1 bar and 350 K using the Berendsen thermostat/barostat<sup>42</sup> with all restraints removed. All pressure coupling was performed semi-isotropically allowing the  $x,y$ -dimensions (the membrane plane) to change independently of the  $z$ -dimension.

During production simulations, pressure was maintained at 1 bar using the Parrinello–Rahman barostat<sup>43</sup> and a 5 ps coupling time. The temperature was maintained using the v-rescale thermostat<sup>44</sup> and a 1 ps coupling time. A time step of 2 fs was used and trajectories were saved every 10 ps. Bonds were constrained using the LINCS algorithm.<sup>45</sup> Short-range interactions were truncated at 1.2 nm with force-switching between 1.0 and 1.2 nm. Long range electrostatics were handled by Particle Mesh Ewald (PME) summation<sup>46</sup> using a 0.12 nm Fourier grid spacing with fourth order interpolation.

**CG Molecular Dynamics.** CG systems were prepared in much the same way as the AA systems, utilizing the CHARMM-GUI to assemble a lipid bilayer using the MARTINI 2.2P (polarizable) force field.<sup>47,48</sup> As MARTINI has an approximately 4:1 mapping of heavy atoms to CG

beads, the carbon tails of DMPC (composed of 14 carbons) can be reasonably described by either 3 or 4 beads. We choose to model DMPC with 4-bead tails (roughly equivalent to 1,2-dipalmitoyl-sn-glycero-3-phosphocholine (DPPC) which has 16 carbons per tail), as the MARTINI model was found to underestimate  $T_m$ , and therefore longer tails would give results more comparable to those of the atomistic system. Trehalose was described by a modified version<sup>49</sup> of the original 6-site model<sup>50</sup> where trehalose–trehalose interactions are decreased to prevent nonphysical aggregation. The mass of the trehalose beads is set to 57 g/mol to yield the proper weight for trehalose, 342 g/mol.

Molecular dynamics simulations were performed using GROMACS 2020.2, as with the atomistic system. As suggested by the CHARMM-GUI output, all systems were first energy minimized in two steps: (1) Steepest descent energy minimization is performed, while all interactions are progressively rescaled from 0.01 to 1 using soft core interactions to resolve any significant clashes. (2) Energy minimization is performed with all interactions switched on. Equilibration consisted of four steps in which the time step was progressively raised from 2 to 20 fs, and membrane restraints were progressively turned off. The last equilibration step was performed for 20 ns at 1 bar and 350 K using the Berendsen thermostat/barostat<sup>42</sup> with all restraints removed. As before, pressure coupling was performed semi-isotropically allowing the  $x,y$ -dimensions (the membrane plane) to change independent of the  $z$ -dimension.

During production simulations, pressure was maintained at 1 bar using the Parrinello–Rahman barostat<sup>43</sup> and a 12 ps coupling time. Temperature was maintained using the v-rescale thermostat<sup>44</sup> and a 1 ps coupling time. A time step of 20 fs was used and trajectories were saved every 10 ps. Bonds were constrained using the LINCS algorithm.<sup>45</sup> Short range interactions were truncated at 1.1 nm. Electrostatics were treated using the reaction-field method ( $\epsilon_{rf} = \infty$ ,  $\epsilon_{bg} = 2.5$ ), as suggested for the polarizable MARTINI force field.<sup>51</sup>

## RESULTS AND DISCUSSION

**Step Annealing Using AA Molecular Dynamics.** We first considered an AA system with a lipid bilayer composed of 128 DMPC lipids in contact with 0, 5, 10, 20, and 40 wt % trehalose solutions prepared as described in the “Methods” section. To investigate the effects of rapid cooling on these systems, we performed stepwise annealing starting at 350 K (well above  $T_m$ ) in which the system was iteratively run for 100 ns at constant temperature before the thermostat temperature was instantaneously dropped by 10 K. This procedure was repeated until the system sampled 250 K (well below  $T_m$ ) for a total run time of 1.1  $\mu$ s for each simulation. In this way, we achieve an average cooling rate of 0.1 K/ns across each simulation while also being able to sample the thermodynamics and kinetics of the system at each 10 K interval. Effects of different cooling rates are discussed in the Supporting Information. We note that while 0.1 K/ns ( $10^8$  K/s) can be considered reasonably slow in the literature of molecular simulation, it is still orders of magnitude faster than cooling rates used for cryopreservation (up to  $10^5$  K/min).<sup>52</sup> Therefore, in terms of relevant experiments, this procedure represents rapid quenching of the system. For all analyses, the first 50 ns of each 100 ns constant temperature block are discarded, and the remaining 50 ns are used for sampling. It should be noted that these sampling windows are not designed

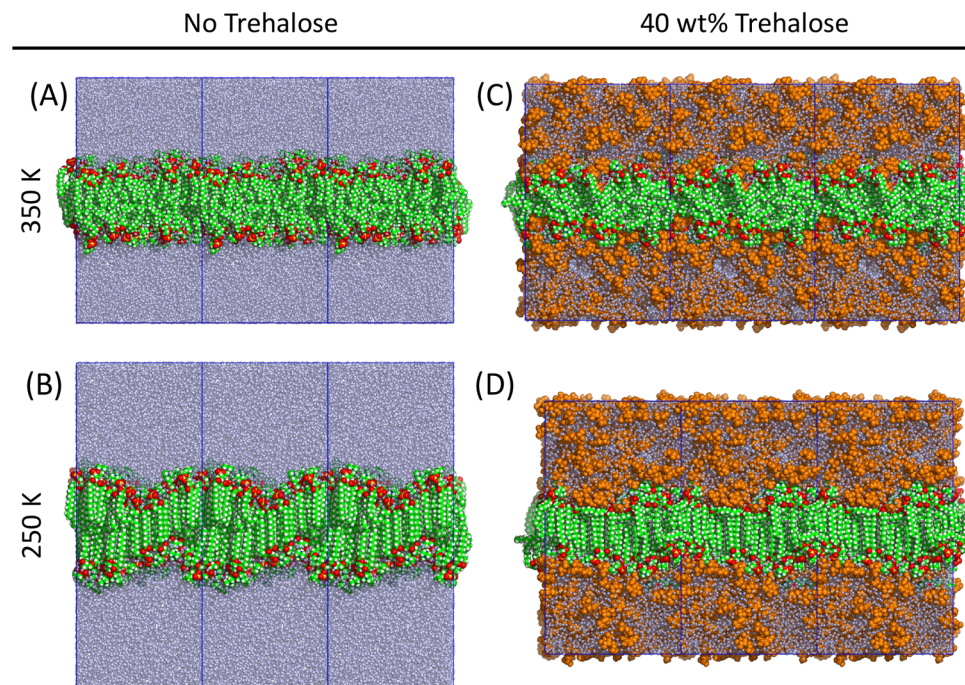


**Figure 1.** Simulation snapshots for the AA system at 350 K containing 0 wt % (A) and 40 wt % trehalose solutions (C) and the same systems at 250 K after step annealing (B, D). Periodic images are shown to highlight the formation of the  $P_\beta$  phase in (B). For the lipids, atoms are shown as follows: carbon in green, oxygen in red, phosphorus in yellow, nitrogen in blue, and hydrogen in white. Trehalose molecules are shown in orange, while water molecules are shown as transparent blue spheres. Visualization done with PyMOL.<sup>53</sup>

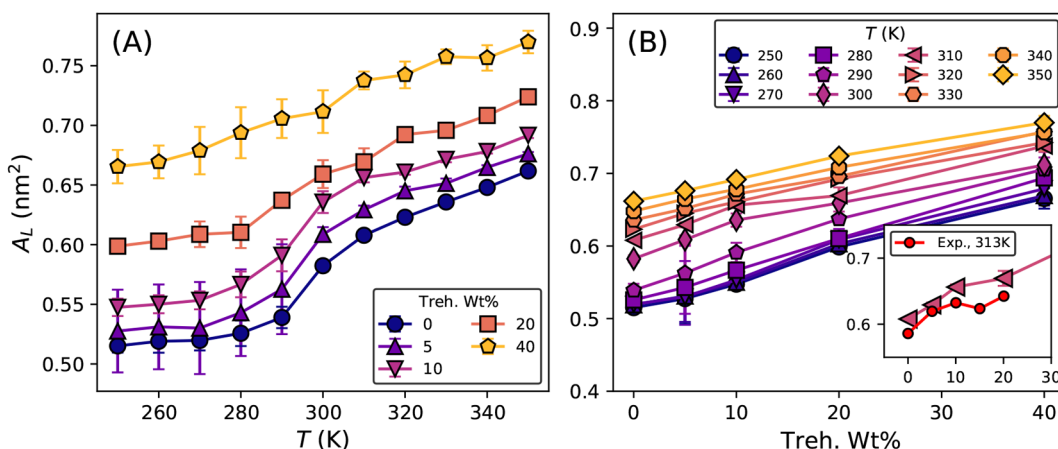


**Figure 2.** Area per lipid,  $A_L$ , for the AA system as a function of temperature (A) and trehalose concentration (B). The inset in (B) shows a comparison of simulation results from this work at 310 K and experimental results from the literature at 313 K.<sup>54</sup> Error bars are  $1.96 \times \text{SE}$  (standard error) determined from three independent simulations.

to reach full equilibrium, especially at and below  $T_m$ . Instead, we aim to relax the system as much as possible under computational constraints before sampling an established metastable state where measured quantities fluctuate around a well-defined mean. See the *Supporting Information* for example time-series data. To obtain error bars, each simulation was performed in triplicate. Simulation snapshots are shown in Figure 1, where a clear formation of the  $P_\beta$  phase (sawtooth pattern) can be seen in Figure 1B.

For each simulation the average area per lipid,  $A_L$ , was calculated by finding the average area of the  $x$ - $y$  plane (parallel to the bilayer) and dividing by the number of lipids. Results are shown in Figure 2 as a function of both temperature and trehalose concentration. Focusing on 0 wt % trehalose,

noticeable nonlinear decrease in  $A_L$  indicates a transition from  $L_\alpha$  to  $P_\beta$  between 290 and 300 K, in good agreement with previous results.<sup>28</sup> The validity of these results is also supported by the agreement between the  $A_L$  measured from these simulations and the  $A_L$  determined experimentally at 313 K, shown in the inset of Figure 2B.

Interestingly, the steepness of this transition decreases with increasing trehalose concentration until the transition disappears at 40 wt % trehalose. From visual inspection of Figure 1D, it can be seen that this is due to a higher prevalence of interdigitation between the upper and lower leaflets, characteristic of the  $P_\beta$  minor domain, which yields a higher  $A_L$ . Furthermore, the softening of the transition with increasing trehalose correlates well with the finding that increased

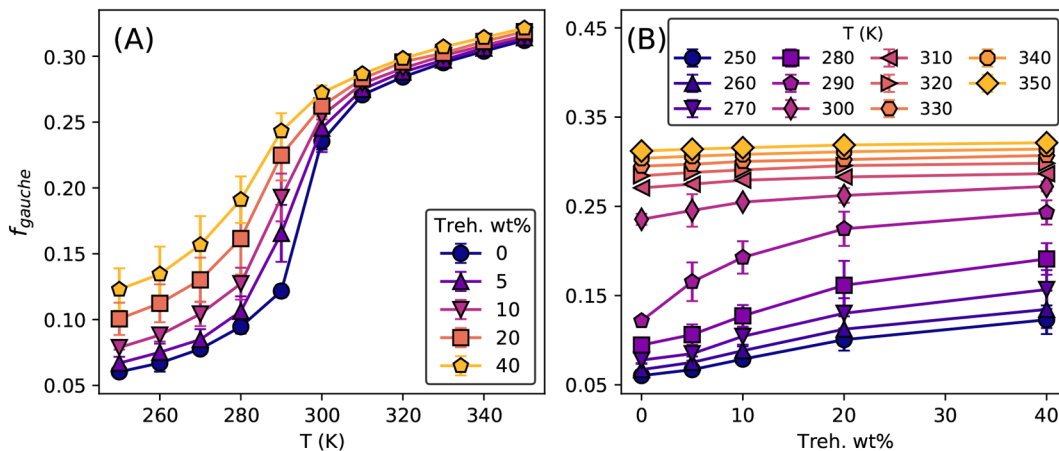


**Figure 3.** Average fraction of *gauche* dihedrals,  $f_{gauche}$ , in the lipid carbon tails for the AA system as a function of temperature,  $T$ , (A) and as a function of trehalose concentration (B). Error bars are  $1.96 \times SE$  determined from three independent simulations.

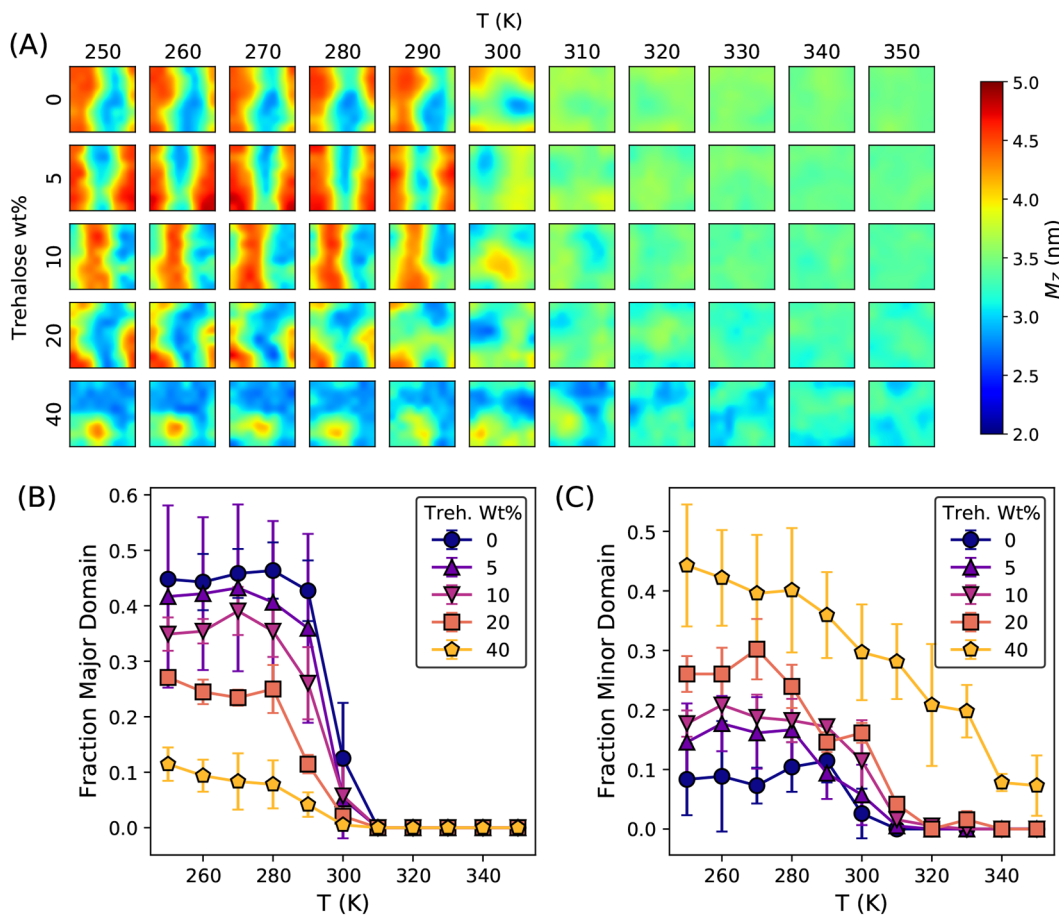


**Figure 4.** Average local membrane thickness,  $M_Z$ , in the AA system for each trehalose concentration and temperature,  $T$ , in the  $x-y$  plane (A). Fraction of the membrane considered to be the major (B) and minor (C) domain of the  $P_\beta$  phase using the membrane thickness from Figure 4A as an order parameter. Error bars are  $1.96 \times SE$  determined from three independent simulations.

trehalose concentration broadens the main peak of the DSC thermogram for similar systems.<sup>24</sup>

In order to probe how trehalose affects the structural properties of the lipid membrane during the  $L_\alpha$  to  $P_\beta$  transition, dihedral angle distributions were calculated using all dihedral angles formed by carbons in the lipid tails. For disordered systems ( $L_\alpha$  phase), there will be a mix of *trans* and *gauche* angles, while ordered systems ( $P_\beta$  and  $L_\beta$  phases) will have a

higher fraction of *trans* angles.<sup>55</sup> Following the method of Leekumjorn and Sum,<sup>56</sup> we define a dihedral angle as *gauche* when it is between  $-120$  and  $120^\circ$ , where  $0^\circ$  is the *cis* angle and  $180^\circ$  (or  $-180^\circ$ ) is the *trans* angle. The average fraction of *gauche* angles,  $f_{gauche}$ , at each temperature is given in Figure 3. As expected, Figure 3A shows a steep decrease in  $f_{gauche}$  for the 0 wt % system as it is cooled from 300 to 290 K (where the  $L_\alpha$  to  $P_\beta$  transition occurs). Above 300 K,  $f_{gauche}$  remains nearly

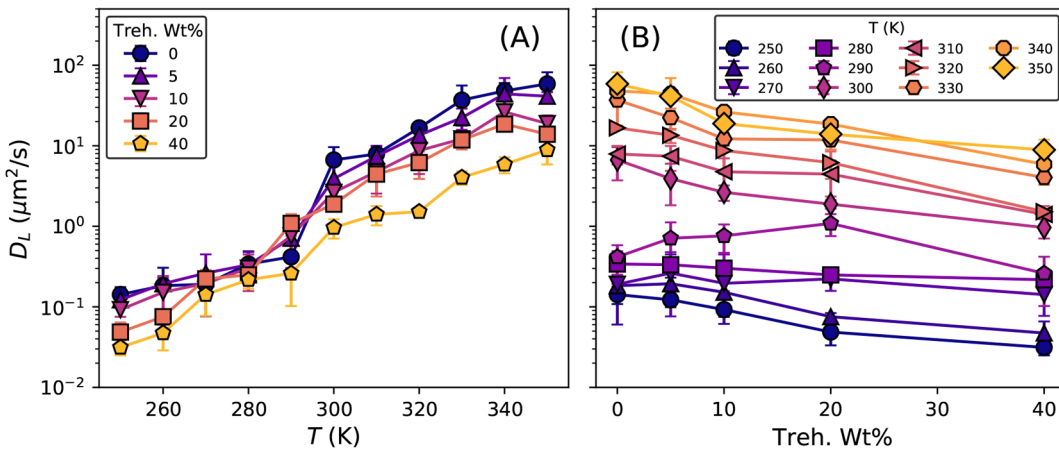


**Figure 5.** Lateral diffusion constant,  $D_L$ , for lipids in the AA system as a function of temperature (A) and trehalose concentration (B). Error bars are  $1.96 \times \text{SE}$  determined from three independent simulations.

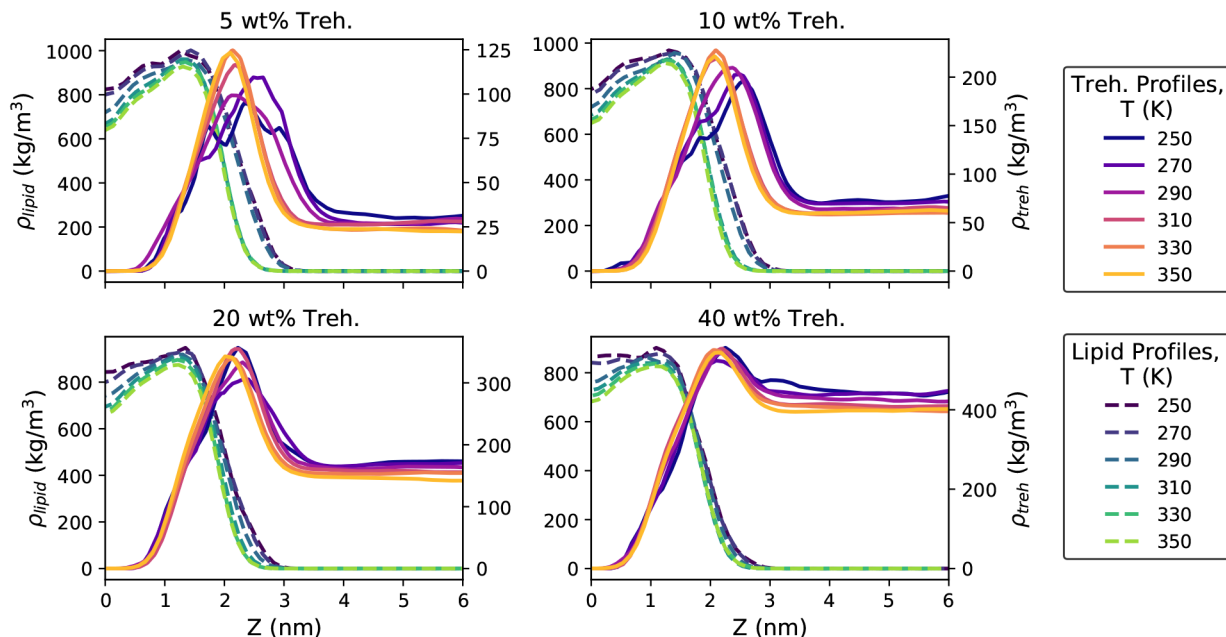


**Figure 6.** Density,  $\rho$ , profiles for 5, 10, 20, and 40 wt % trehalose averaged along the  $z$  direction (perpendicular to the membrane) for the AA system. The membrane is centered at  $z = 0$ . Profiles for the lipids are shown as dashed lines and correspond to the left vertical axis in each plot. Profiles for trehalose are shown as solid lines and correspond to the right vertical axis in each plot.

constant as the trehalose concentration is increased. However, for temperatures below 300 K, increasing the trehalose concentration increases  $f_{\text{gauche}}$  (see Figure 3B), indicating that the addition of trehalose causes progressive disordering of the lipid membrane at low temperatures. Measurement of the lipid NMR order parameters also showed increased disorder with increased trehalose concentration (see the Supporting Information for details.)

The formation of the  $P_\beta$  phase was further investigated by computing the local membrane thickness,  $M_Z$ , as defined by the vertical ( $z$ -axis) distance between phosphate groups of the upper and lower leaflets. Average values of  $M_Z$  were obtained for each sampling window using an  $8 \times 8$  grid ( $x-y$  plane), shown in Figure 4A. At high temperatures and low trehalose concentration,  $M_Z$  is constant across the simulation cell, indicating the  $L_\alpha$  phase. Near 300 K, variation in  $M_Z$  starts to appear and a ripple becomes visible. As  $M_Z$  takes on

significantly different values in the major and minor domains of the  $P_\beta$  phase (due to interdigitation in the minor domain),<sup>28</sup> we use it as an order parameter to roughly define the thick region (where  $M_Z > 4.0$  nm) as the major domain and the thin region (where  $M_Z < 3.0$  nm) as the minor domain. Under these definitions, it can be seen from Figure 4A that, below 300 K, as the trehalose concentration is increased, the minor domain becomes more prevalent until almost none of the major domain remains. This can be seen quantitatively in Figure 4B,C, where the fraction of the cell classified as the  $P_\beta$  major/minor domain is shown. We note that at higher trehalose concentrations, especially 40 wt %, membrane thinning was observed above 300 K (see Figure 4A), suggesting that even above  $T_m$  trehalose increases leaflet interdigitation.  $M_Z$  was also used, in combination with  $A_L$ , to calculate the average volume per lipid,  $V_L$ , which was found to

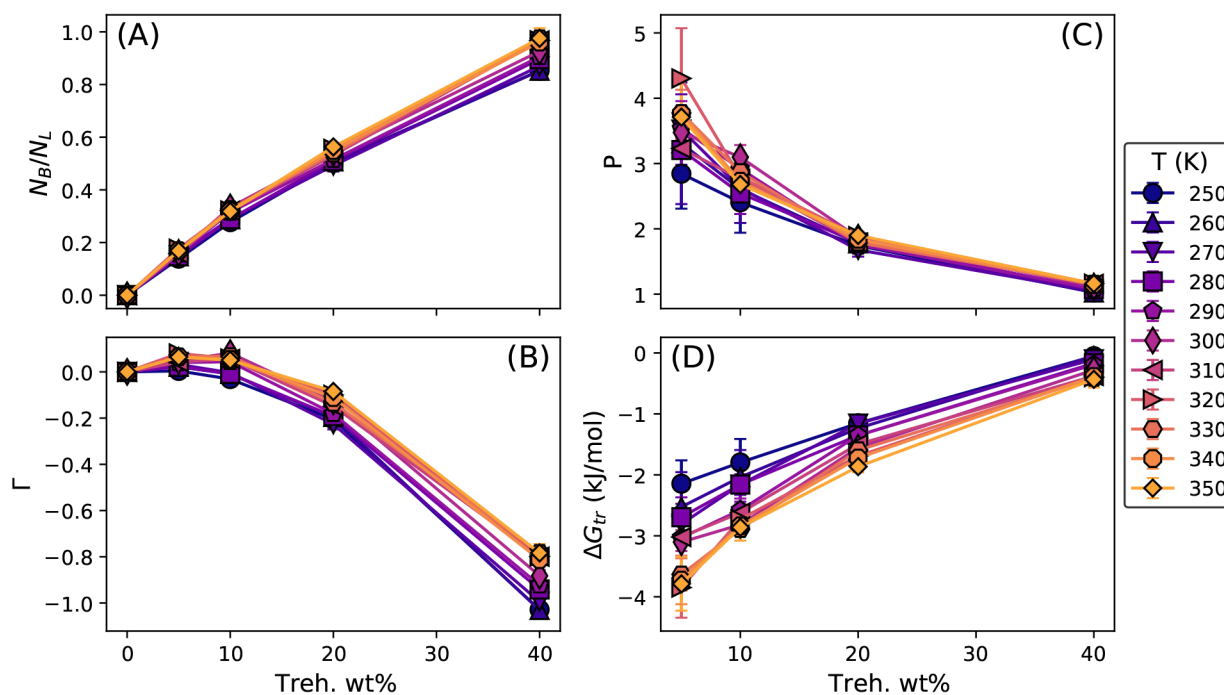


**Figure 7.** Trehalose binding analysis for the AA system: (A) Number of bound trehalose molecules per lipid,  $N_B/N_L$ , (B) net affinity,  $\Gamma$ , of trehalose for the membrane, (C) partition coefficient,  $P$ , and (D) free energy of transfer for trehalose moving from the bulk to the interface,  $\Delta G_{tr}$ . Error bars are  $1.96 \times \text{SE}$  determined from three independent simulations.

follow the same trends observed for  $A_L$  (see the *Supporting Information* for details).

We then investigated the kinetic effect of trehalose on the lateral diffusion coefficient,  $D_L$ , for lipids in the bilayer. Here,  $D_L$  was calculated from the slope of the lateral mean-square displacement (MSD) curve of the lipid headgroups (see the *Supporting Information* for details of this calculation). Results are shown in Figure 5. At 310 K,  $D_L = 7.90 \pm 2.05 \mu\text{m}^2/\text{s}$  for the pure water system, which is in good agreement with  $9.16 \mu\text{m}^2/\text{s}$  determined experimentally.<sup>57</sup> Again, we see a noticeable transition between 290 and 300 K for 0 wt % trehalose where  $D_L$  steeply decreases as expected due to the  $L_\alpha$  to  $P_\beta$  transition. This transition is damped as the trehalose concentration is increased; however, this effect is overwhelmed by the general decrease or plateau (within error bars) in  $D_L$  at most temperatures as the concentration of trehalose is increased (Figure 5B). This is not surprising as trehalose significantly increases the viscosity of the solvent.<sup>58</sup>

Spatial interactions between trehalose and the membrane were then characterized by calculating density profiles, shown in Figure 6. Work by Kapla et al.<sup>15</sup> showed the density of trehalose molecules far from the membrane decaying to zero; however, we find that while the concentration of trehalose does plateau far from the membrane, it never decays to zero. This is due to our use of the adjusted trehalose parameters suggested by Lay et al.<sup>36</sup> which decrease the trehalose-trehalose interaction strength to better match osmotic pressure measurements. As a result, the trehalose molecules in our simulations do not overaggregate and thereby maintain a more realistic solubility throughout the simulation cell at ambient temperature (evidence of aggregation without the adjusted trehalose parameters is shown in the *Supporting Information*). Several results are notable from Figure 6: (1) There is a strong overlap between the membrane profile and the trehalose profile at all temperatures, indicating that trehalose intercalates between the

lipid headgroups (visible in Figure 1) as reported previously.<sup>24</sup> (2) At low trehalose concentrations (5 and 10 wt %), the lipid profile shifts slightly outward at low temperatures as a result of the  $L_\alpha$  to  $P_\beta$  transition, where alignment of the lipid tails in the major domain increases the bilayer thickness. Simultaneously, the trehalose profile also shifts out and develops a shoulder as trehalose binds to the major and minor domains at different distances from the bilayer center. At higher trehalose concentrations (20 and 40 wt %), this shift disappears in agreement with our results presented above which indicate that trehalose suppresses the formation of the  $P_\beta$  major domain at high concentration. (3) In general, trehalose concentration near the membrane decreases with decreasing temperature, accompanied by a corresponding increased concentration in the bulk. This is most likely due to the decreased lipid headgroup spacing at the surface of the membrane as lipids transition from a more mobile state at high temperatures to a more restricted and tightly packed structure at low temperatures, thereby decreasing the number of favorable binding sites for trehalose to interact with the membrane interface. Free energy profiles for the AA and CG systems (derived from the density profiles shown in Figures 6 and 12) are given in the *Supporting Information*.

Further analysis of the trehalose–membrane interactions is provided by considering the two-state binding model proposed by Kapla et al.<sup>15</sup> This model considers the trehalose molecules to be either in a bound state (near the membrane) or a free state (away from the membrane). We consider all trehalose molecules with a center of mass within  $r_c = 1 \text{ nm}$  of the lipid phosphate atoms to be bound, with the average number of bound trehalose molecules denoted  $N_B$ . This definition is useful as it is consistent regardless of changes in the bilayer thickness and easily transferable to CG simulations discussed later in this work. The net affinity,  $\Gamma$ , between  $N$  trehalose

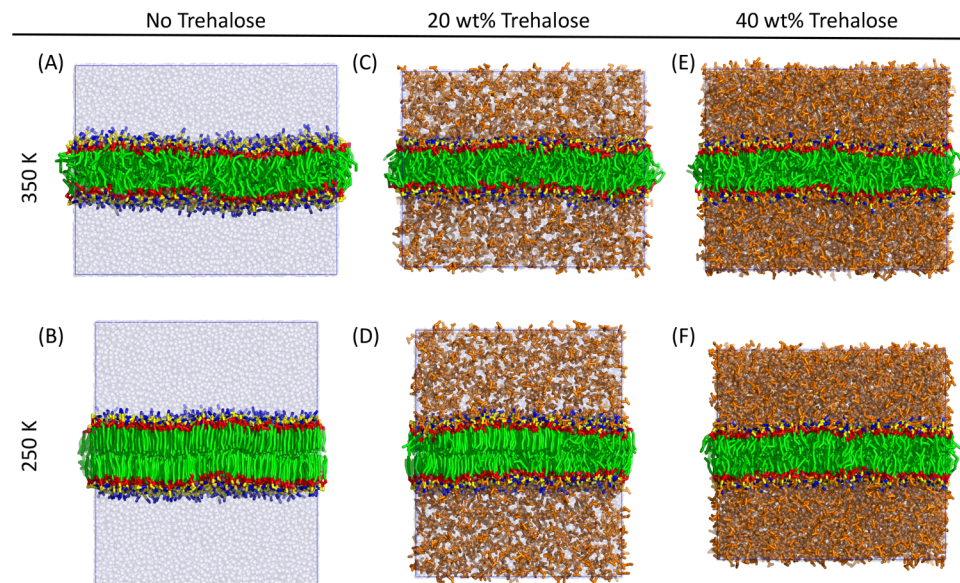


**Figure 8.** Simulation snapshots for the CG system at 350 K for 0 (A), 20 (C), and 40 (E) wt % trehalose, and the same systems at 250 K after step annealing (B, D, F). For the lipids, atoms are shown as follows: carbon groups in green, oxygen in red, phosphorus in yellow, and nitrogen in blue. Trehalose molecules are shown in orange, while water molecules are shown as transparent blue spheres. Visualization was done with PyMOL.<sup>53</sup>

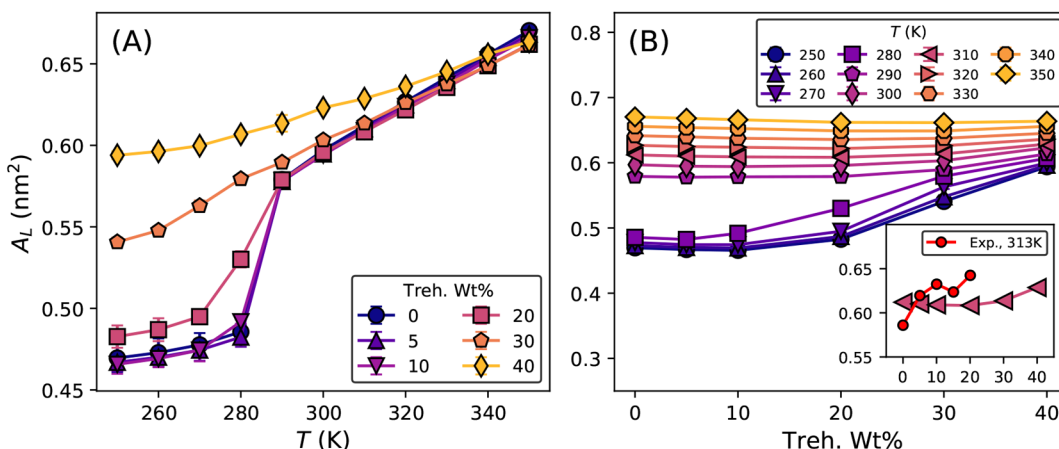


**Figure 9.** Area per lipid,  $A_L$ , for the CG system as a function of temperature (A) and trehalose concentration (B). Inset in (B) shows a comparison of simulation results from this work at 310 K and experimental results from the literature at 313 K.<sup>54</sup> Error bars are  $1.96 \times \text{SE}$  determined from three independent simulations.

molecules and a membrane composed of  $N_L$  lipids is then given as<sup>15</sup>

$$\Gamma = (N_B - N_F)/N_L = (2N_B - N)/N_L \quad (1)$$

Here,  $N_F$  is the number of free trehalose molecules, equal to  $N - N_B$ . Since this definition for  $\Gamma$  does not account for the quantity of solvent (i.e., the  $z$ -dimension of our system), one must remember that systems of different size will yield different  $\Gamma$  (as discussed by Kapla et al.<sup>15</sup>). Results are shown in Figure 7, where the curve for  $\Gamma$  is nonmonotonic, in qualitative agreement with results reported by Andersen et al.<sup>54</sup> The partition coefficient,  $P$ , and the free energy of transfer for trehalose moving from the bulk to the interface,  $\Delta G_{\text{tr}}$  can then be calculated from the following:

$$P = \frac{C_B}{C_F} = \frac{N_B/Z_B}{N_F/Z_F} \quad (2)$$

$$\Delta G_{\text{tr}} = -k_B T \ln(P) \quad (3)$$

$C_B$  and  $C_F$  are the concentrations of trehalose in the bound and free states, respectively, and  $k_B$  is the Boltzmann constant. These values are determined by assuming that the ratio of the bound and free volumes are given by a ratio of the  $z$ -dimension of the bound region,  $Z_B = 4r_c = 4$  nm (for both side of the membrane), and the  $z$ -dimension of the free region,  $Z_F = L_Z - M_Z - 2r_c$ . Here,  $L_Z$  is the  $z$ -dimension of the simulation cell and  $M_Z$  is the thickness of the membrane. Results are shown in Figure 7, where we find that  $P$  ranges from approximately 4 at low concentrations, to roughly 1 at high concentrations. At low concentrations, these values are higher than the experimentally reported partition coefficients which range from 0.6 to 2.5,<sup>54</sup> but some deviation is expected as the “bulk” region of the simulations is still rather confined (<10 nm between periodic images of the membrane) compared to experiment where the ratio of water molecules to lipids is an order of magnitude greater.

**Step Annealing Using CG Molecular Dynamics.** In order to study larger length scales at a much reduced

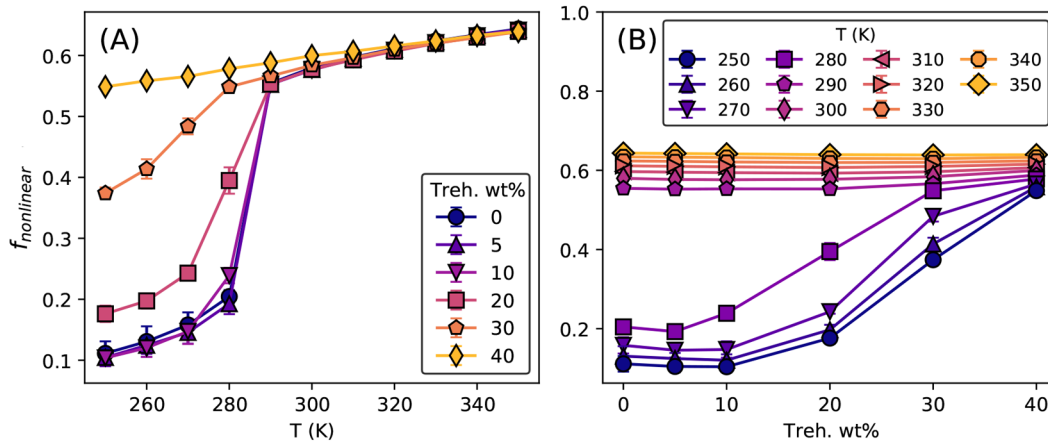


**Figure 10.** Average fraction of nonlinear lipid tail angles,  $f_{\text{nonlinear}}$ , for the CG system as a function of temperature,  $T$ , (A) and as a function of trehalose concentration (B). Error bars are  $1.96 \times \text{SE}$  determined from three independent simulations.

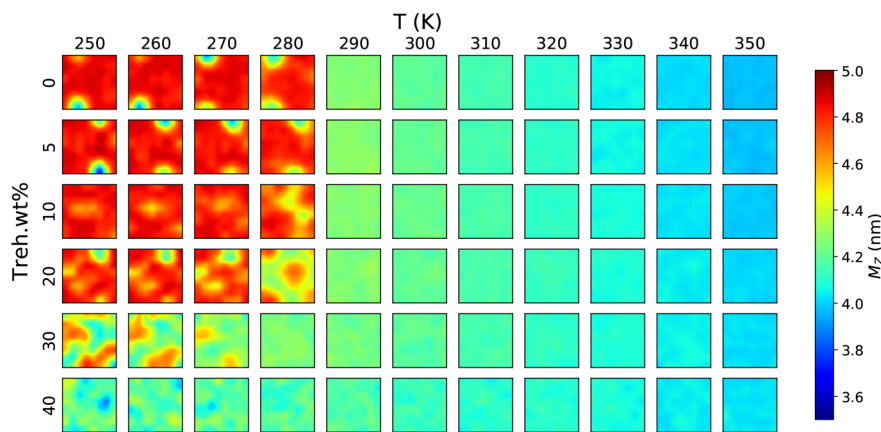


**Figure 11.** Average local membrane thickness,  $M_Z$ , in the CG system for each trehalose concentration and temperature,  $T$ .

computational cost, the MARTINI force field was used to describe a CG bilayer of 1024 lipids in contact with a trehalose/water solution as described in the “Methods” section. Simulation snapshots of the CG system are provided in Figure 8. Our use of a decreased trehalose–trehalose interaction potential as suggested by Schmalhorst et al.<sup>49</sup> avoids the overaggregation of trehalose molecules observed by Kapla et al.<sup>25</sup>

Following the same stepwise annealing used for the AA system, we found that the CG bilayer transitioned directly from  $L_\alpha$  to  $L_\beta$  between 290 and 280 K without forming a stable  $P_\beta$  phase at any temperature. This may be explained by recalling that  $P_\beta$  eventually transitions to  $L_\beta$  at low temperatures<sup>26,28</sup> and that the persistence of the  $P_\beta$  phase in the AA system is a result of the system kinetics becoming arrested at low temperatures. However, the lack of atomic detail in the CG system leads to greater lipid mobility (see the Supporting Information for details); therefore, the system is able to fully relax to the  $L_\beta$  phase.

Even with this difference, the CG system qualitatively reproduces important aspects of the behavior of the AA system. For example, Figure 9A shows that increasing the trehalose concentration suppresses the transition to lower  $A_L$  at low temperatures, as was observed for the AA system. Additionally, Figure 9B shows that for temperatures below 300 K  $A_L$  increases with trehalose concentration as is observed

in the AA system. However, it should be noted that above 300 K  $A_L$  is nearly constant as a function of trehalose concentration in the CG system, whereas  $A_L$  increases with addition of trehalose at all temperatures in the AA system. A benefit of the larger simulation cell used in the CG system is that reasonably accurate measurements of the membrane compressibility modulus,  $K_A$ , can be obtained from fluctuations in  $A_L$ . Details of this calculation and the corresponding results are provided in the Supporting Information.

In order to compare with the results presented above for the fraction of *gauche* isomers in the AA system, we computed distributions for lipid tail bond angles,  $\Theta$ , in the CG system (since the CG system has no equivalent dihedral angles). Specifically,  $\Theta$  is the angle formed between each pair of consecutive bonds in the tails of each lipid. In the more disordered fluid phase,  $L_\omega$ ,  $\Theta$  has a broad distribution between 60 and 180°, with a maximum between 140 and 150° (see the Supporting Information for an example of  $\Theta$  distributions). In the more ordered  $L_\beta$  phase (where the lipid tails adopt more linear configurations),  $\Theta$  has a narrower distribution closer to 180°. Therefore, we define the quantity  $f_{\text{nonlinear}}$  as the fraction of  $\Theta$  observations less than 150° (chosen as the angle at which distributions of  $\Theta$  in the  $L_\alpha$  and  $L_\beta$  phase intersect). As such,  $f_{\text{nonlinear}}$  should be qualitatively comparable to  $f_{\text{gauche}}$ . Results are shown in Figure 10, where the similarities to results for the AA system (Figure 3) are apparent. We see a similar decrease in

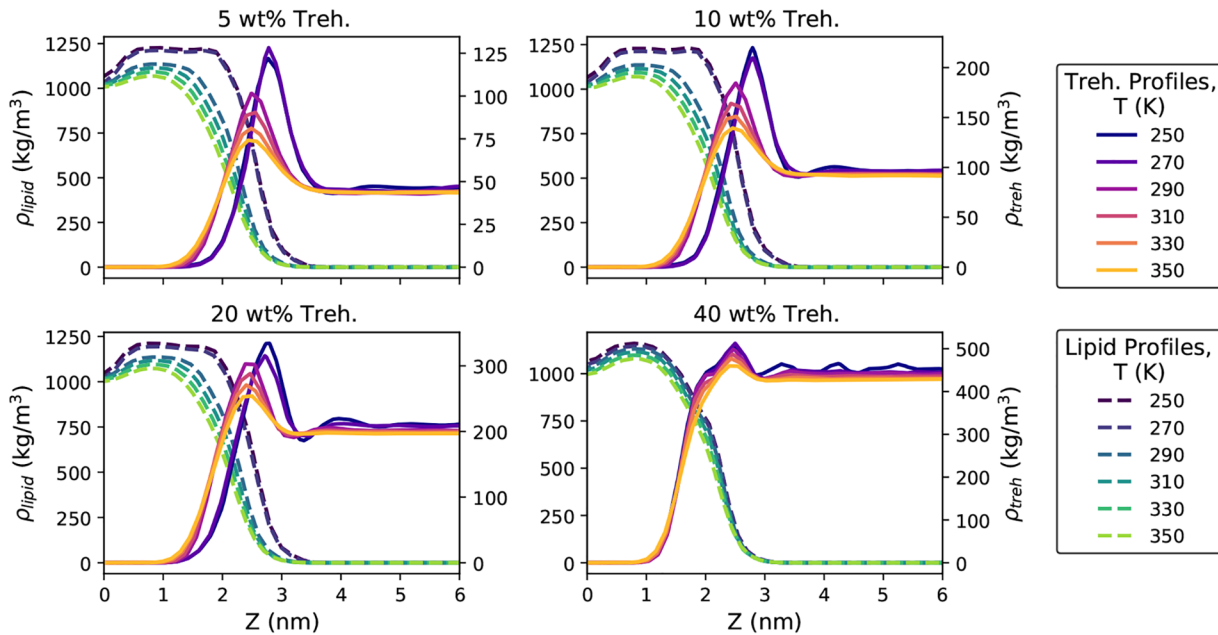


**Figure 12.** Density,  $\rho$ , profiles for 5, 10, 20, and 40 wt % trehalose averaged along the  $z$  direction (perpendicular to the membrane) for the CG system. The membrane is centered at  $z = 0$ . Profiles for the lipids are shown as dashed lines and correspond to the left vertical axis in each plot. Profiles for trehalose are shown as solid lines and correspond to the right vertical axis in each plot.

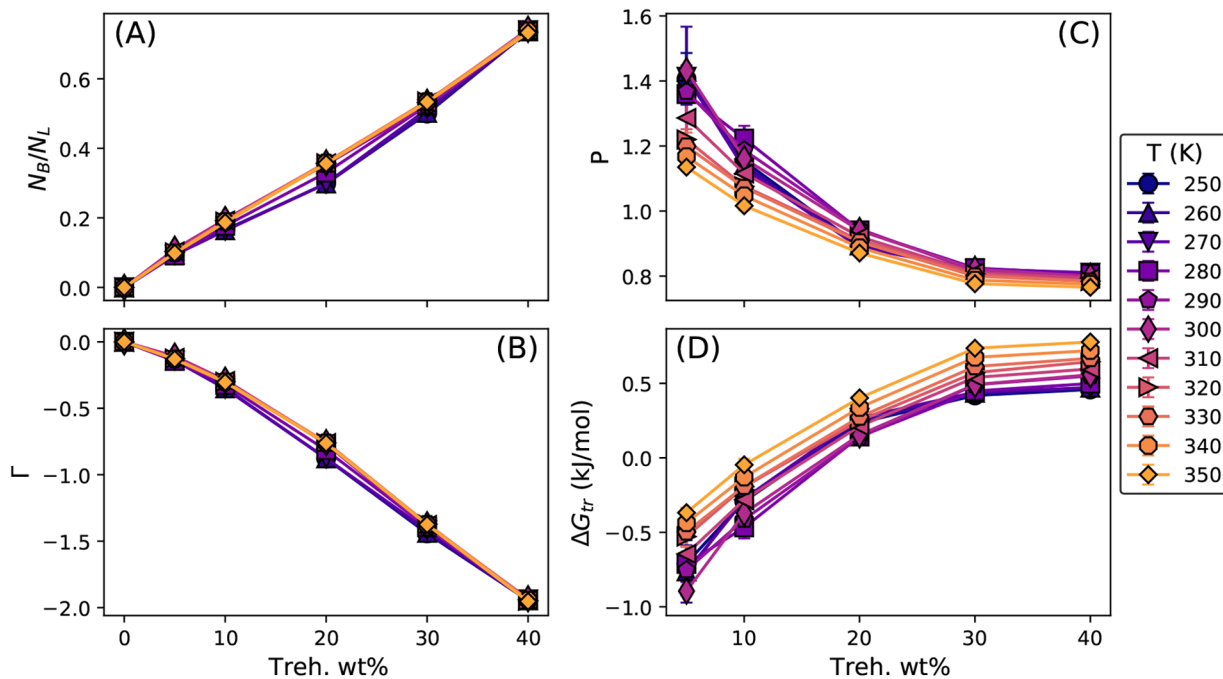


**Figure 13.** Trehalose binding analysis for the CG system: (A) number of bound trehalose molecules per lipid,  $N_B/N_L$ , (B) net affinity,  $\Gamma$ , of trehalose for the membrane, (C) partition coefficient,  $P$ , and (D) free energy of transfer for trehalose moving from the bulk to the interface,  $\Delta G_{tr}$ . Error bars are  $1.96 \times SE$  determined from three independent simulations.

$f_{\text{nonlinear}}$  near the  $L_\alpha$  to  $L_\beta$  transition (280–290 K) in Figure 10A as was seen for  $f_{\text{gauche}}$  near the  $L_\alpha$  to  $P_\beta$  transition in Figure 3A. Additionally,  $f_{\text{nonlinear}}$  increases with addition of trehalose (Figure 10B) for temperatures below the phase transition, just as was seen with  $f_{\text{gauche}}$  (see Figure 3B). These results therefore suggest that trehalose increases lipid disorder in the CG system, just as it did in the AA system.

The effects of trehalose on the transition from the  $L_\alpha$  to the  $L_\beta$  phase in the CG system is also apparent from  $M_Z$  as shown

in Figure 11. At concentrations of 0 or 5 wt % trehalose, a clear transition occurs between 290 and 280 K where, excluding small defects, the entire system transitions uniformly to a larger  $M_Z$ , indicating the formation of the  $L_\beta$  phase (and confirming the absence of the  $P_\beta$  phase as no continuous regions of membrane thinning are observed). For 10 and 20 wt % trehalose, patches of  $L_\alpha$  remain at 280 K, but these mainly disappear at lower temperatures. At 30 wt % trehalose, the transition to  $L_\beta$  is clearly inhibited at 280 K, but regions of  $L_\beta$

start to form at 270 K. Finally, at 40 wt % trehalose, the formation of  $L_\beta$  is fully suppressed and  $M_Z$  at 250 K is very similar to the  $M_Z$  observed at 300 K.

Density profiles for the CG system are shown in Figure 12, where the trehalose density is clearly enhanced near the membrane interface, especially at low concentrations. As with the AA system, higher concentrations of trehalose suppress the low temperature transition to a thicker membrane, yielding a membrane profile nearly the same at 250 and 350 K for 40 wt % trehalose. Additionally, the same two-state binding analysis discussed for the AA system was performed for the CG system.  $\Gamma$  was found to be lower for the CG system (Figure 13), with  $\Gamma \leq 0$  for all concentrations. Correspondingly,  $P$  was also lower with values closer to those reported from experiment ( $P = 0.6\text{--}2.5$ ).<sup>54</sup> Since the CG system has roughly the same  $z$ -dimensions as the AA system (it is only larger in the  $x/y$ -dimensions parallel to the membrane),  $Z_B/Z_F$  is roughly the same. Therefore, this difference is not due to the system size, rather it is most likely due to the lack of explicit hydrogen bonding interactions in the CG model.

## CONCLUSION

In this work, all-atom (AA) and coarse-grained (CG) molecular dynamics simulations were used to probe the effect of trehalose on a model DMPC lipid membrane under rapid cooling. Below 300 K, the AA system was found to transition from the disordered liquid crystalline phase,  $L_\alpha$  to the more ordered ripple phase,  $P_\beta$ . The addition of trehalose damped this transition, yielding an increased area per lipid,  $A_L$ , at and below the transition. Measurement of the local membrane thickness,  $M_Z$ , showed that this increase in  $A_L$  was due to trehalose suppressing the formation of the major domain of the  $P_\beta$  phase (similar to the gel phase,  $L_\beta$ ) in favor of the interdigitated minor domain (which has a lower  $M_Z$  and higher  $A_L$  than the major domain). The addition of trehalose also increased the fraction of *gauche* isomers in the AA system, indicating that trehalose increases the lipid disorder in the membrane. Density profiles indicate that trehalose strongly interacts with the lipid membrane surface in the AA systems. Further analysis using a two-state model revealed preferential binding of trehalose to the membrane interface, with partition coefficients (between the interface and bulk solution) ranging from  $\approx 4$  at low trehalose concentrations to  $\approx 1$  at high trehalose concentrations.

The CG system does not show formation of the  $P_\beta$  phase (as observed in the AA system), but it instead transitions directly from the  $L_\alpha$  to  $L_\beta$  phase. However, many similarities are observed between the CG and AA systems. Addition of trehalose to the CG system leads to a higher  $A_L$  at low temperatures, as in the AA system. Measurement of  $M_Z$  for the CG system shows that this is due to trehalose suppressing the formation of the  $L_\beta$  phase (which has a higher  $M_Z$  and lower  $A_L$  than the  $L_\alpha$  phase), similar to trehalose suppressing the  $P_\beta$  phase in the AA system. Increased lipid disorder was also observed in the CG system upon addition of trehalose as measured by an increased fraction of nonlinear lipid tails. Partition coefficients were found to be lower for the CG system than those in the AA, ranging from  $\approx 1.4$  at low concentrations to  $\approx 0.8$  at high concentrations, likely due to the lack of explicit hydrogen bonding in the CG model.

Given the importance of designing next-generation cryopreservatives that stabilize lipid membranes, we hope that this work inspires future molecular studies of small

molecules (especially other saccharides) interacting with membranes. A natural extension of this work would be to investigate the effects of trehalose on more complex membranes with compositions closer to those found in biological systems. Furthermore, our demonstration of the reasonable behavior in the CG system should serve as encouragement to study more complicated and larger length scale structures, such as transmembrane protein assemblies or vesicles.

## ASSOCIATED CONTENT

### Supporting Information

The Supporting Information is available free of charge at <https://pubs.acs.org/doi/10.1021/acs.jpcb.1c02575>.

List of the systems studied in this work, additional analysis, and data from simulations using different force field parameters and system sizes (PDF)

## AUTHOR INFORMATION

### Corresponding Author

Pablo G. Debenedetti – Department of Chemical and Biological Engineering, Princeton University, Princeton, New Jersey 08544, United States;  [orcid.org/0000-0003-1881-1728](https://orcid.org/0000-0003-1881-1728); Email: [pdebene@princeton.edu](mailto:pdebene@princeton.edu)

### Authors

Daniel J. Kozuch – Department of Chemical and Biological Engineering, Princeton University, Princeton, New Jersey 08544, United States;  [orcid.org/0000-0002-9671-8396](https://orcid.org/0000-0002-9671-8396)

Frank H. Stillinger – Department of Chemistry, Princeton University, Princeton, New Jersey 08544, United States;  [orcid.org/0000-0002-1225-8186](https://orcid.org/0000-0002-1225-8186)

Complete contact information is available at: <https://pubs.acs.org/doi/10.1021/acs.jpcb.1c02575>

### Notes

The authors declare no competing financial interest.

## ACKNOWLEDGMENTS

This material is based upon work supported by the National Science Foundation Graduate Research Fellowship under Grant No. DGE-1656466 awarded to D.J.K.

## REFERENCES

- (1) Crowe, J. H.; Crowe, L. M.; Carpenter, J. F.; Aurell Wistrom, C. Stabilization of dry phospholipid bilayers and proteins by sugars. *Biochem. J.* **1987**, *242*, 1–10.
- (2) Lambruschini, C.; Relini, A.; Ridi, A.; Cordone, L.; Gliozzi, A. Trehalose interacts with phospholipid polar heads in Langmuir monolayers. *Langmuir* **2000**, *16*, 5467–5470.
- (3) Al-Ayoubi, S. R.; Schinkel, P. K. F.; Berghaus, M.; Herzog, M.; Winter, R. Combined effects of osmotic and hydrostatic pressure on multilamellar lipid membranes in the presence of PEG and trehalose. *Soft Matter* **2018**, *14*, 8792–8802.
- (4) Dhaliwal, A.; Khondker, A.; Alsop, R.; Rheinstädter, M. C. Glucose can protect membranes against dehydration damage by inducing a glassy membrane state at low hydrations. *Membranes (Basel, Switz.)* **2019**, *9*, 15.
- (5) Crowe, J. H.; Carpenter, J. F.; Crowe, L. M. The Role of Vitrification in Anhydrobiosis. *Annu. Rev. Physiol.* **1998**, *60*, 73–103.
- (6) Eroglu, A.; Russo, M. J.; Bieganski, R.; Fowler, A.; Cheley, S.; Bayley, H.; Toner, M. Intracellular trehalose improves the survival of cryopreserved mammalian cells. *Nat. Biotechnol.* **2000**, *18*, 163–167.

- (7) Kaushik, J. K.; Bhat, R. Why Is Trehalose an Exceptional Protein Stabilizer? *J. Biol. Chem.* **2003**, *278*, 26458–26465.
- (8) Wei, Y.; Li, C.; Zhang, L.; Xu, X. Design of novel cell penetrating peptides for the delivery of trehalose into mammalian cells. *Biochim. Biophys. Acta, Biomembr.* **2014**, *1838*, 1911–1920.
- (9) Athurupana, R.; Takahashi, D.; Ioki, S.; Funahashi, H. Trehalose in glycerol-free freezing extender enhances post-thaw survival of boar spermatozoa. *J. Reprod. Dev.* **2015**, *61*, 205–210.
- (10) Sum, A. K.; Faller, R.; de Pablo, J. J. Molecular Simulation Study of Phospholipid Bilayers and Insights of the Interactions with Disaccharides. *Biophys. J.* **2003**, *85*, 2830–2844.
- (11) Pereira, C. S.; Lins, R. D.; Chandrasekhar, I.; Freitas, L. C. G.; Hünenberger, P. H. Interaction of the Disaccharide Trehalose with a Phospholipid Bilayer: A Molecular Dynamics Study. *Biophys. J.* **2004**, *86*, 2273–2285.
- (12) Villarreal, M. A.; Díaz, S. B.; Disalvo, E. A.; Montich, G. G. Molecular Dynamics Simulation Study of the Interaction of Trehalose with Lipid Membranes. *Langmuir* **2004**, *20*, 7844–7851.
- (13) Doxastakis, M.; Sum, A. K.; de Pablo, J. J. Modulating Membrane Properties: The Effect of Trehalose and Cholesterol on a Phospholipid Bilayer. *J. Phys. Chem. B* **2005**, *109*, 24173–24181.
- (14) Skibinsky, A.; Venable, R. M.; Pastor, R. W. A Molecular Dynamics Study of the Response of Lipid Bilayers and Monolayers to Trehalose. *Biophys. J.* **2005**, *89*, 4111–4121.
- (15) Kapla, J.; Wohlert, J.; Stevensson, B.; Engström, O.; Widmalm, G.; Maliniak, A. Molecular Dynamics Simulations of Membrane–Sugar Interactions. *J. Phys. Chem. B* **2013**, *117*, 6667–6673.
- (16) Kapla, J.; Engström, O.; Stevensson, B.; Wohlert, J.; Widmalm, G.; Maliniak, A. Molecular dynamics simulations and NMR spectroscopy studies of trehalose–lipid bilayer systems. *Phys. Chem. Chem. Phys.* **2015**, *17*, 22438–22447.
- (17) Kumar, A.; Cincotti, A.; Aparicio, S. Insights into the interaction between lipid bilayers and trehalose aqueous solutions. *J. Mol. Liq.* **2020**, *314*, 113639.
- (18) Leekumjorn, S.; Sum, A. K. Molecular Dynamics Study on the Stabilization of Dehydrated Lipid Bilayers with Glucose and Trehalose. *J. Phys. Chem. B* **2008**, *112*, 10732–10740.
- (19) Pereira, C. S.; Hünenberger, P. H. Effect of Trehalose on a Phospholipid Membrane under Mechanical Stress. *Biophys. J.* **2008**, *95*, 3525–3534.
- (20) Taylor, M. J.; Weegman, B. P.; Baicu, S. C.; Giwa, S. E. New Approaches to Cryopreservation of Cells, Tissues, and Organs. *Transfus. Med. Hemotherapy* **2019**, *46*, 197–215.
- (21) Gautier, J.; Passot, S.; Pénaud, C.; Guillemin, H.; Cenard, S.; Lieben, P.; Fonseca, F. A low membrane lipid phase transition temperature is associated with a high cryotolerance of *Lactobacillus delbrueckii* subspecies *bulgaricus* CFL1. *J. Dairy Sci.* **2013**, *96*, 5591–5602.
- (22) Zhang, M.; Oldenhof, H.; Sieme, H.; Wolkers, W. F. Freezing-induced uptake of trehalose into mammalian cells facilitates cryopreservation. *Biochim. Biophys. Acta, Biomembr.* **2016**, *1858*, 1400–1409.
- (23) Crowe, L. M.; Crowe, J. H. Solution effects on the thermotropic phase transition of unilamellar liposomes. *Biochim. Biophys. Acta, Biomembr.* **1991**, *1064*, 267–274.
- (24) Ohtake, S.; Schebor, C.; de Pablo, J. J. Effects of trehalose on the phase behavior of DPPC–cholesterol unilamellar vesicles. *Biochim. Biophys. Acta, Biomembr.* **2006**, *1758*, 65–73.
- (25) Kapla, J.; Stevensson, B.; Maliniak, A. Coarse-Grained Molecular Dynamics Simulations of Membrane–Trehalose Interactions. *J. Phys. Chem. B* **2016**, *120*, 9621–9631.
- (26) Kranenburg, M.; Smit, B. Phase Behavior of Model Lipid Bilayers. *J. Phys. Chem. B* **2005**, *109*, 6553–6563.
- (27) Eeman, M.; Deleu, M. From biological membranes to biomimetic model membranes. *Biotechnol. Agron. Société Environ.* **2010**, *14*, 719–736.
- (28) Khakbaz, P.; Klauda, J. B. Investigation of phase transitions of saturated phosphocholine lipid bilayers via molecular dynamics simulations. *Biochim. Biophys. Acta, Biomembr.* **2018**, *1860*, 1489–1501.
- (29) de Vries, A. H.; Yefimov, S.; Mark, A. E.; Marrink, S. J. Molecular structure of the lecithin ripple phase. *Proc. Natl. Acad. Sci. U. S. A.* **2005**, *102*, 5392–5396.
- (30) Akabori, K.; Nagle, J. F. Structure of the DMPC lipid bilayer ripple phase. *Soft Matter* **2015**, *11*, 918–926.
- (31) Jo, S.; Kim, T.; Iyer, V. G.; Im, W. CHARMM-GUI: A web-based graphical user interface for CHARMM. *J. Comput. Chem.* **2008**, *29*, 1859–1865.
- (32) Jo, S.; Lim, J. B.; Klauda, J. B.; Im, W. CHARMM-GUI Membrane Builder for Mixed Bilayers and Its Application to Yeast Membranes. *Biophys. J.* **2009**, *97*, 50–58.
- (33) Lee, J.; Cheng, X.; Swails, J. M.; Yeom, M. S.; Eastman, P. K.; Lemkul, J. A.; Wei, S.; Buckner, J.; Jeong, J. C.; Qi, Y.; et al. CHARMM-GUI Input Generator for NAMD, GROMACS, AMBER, OpenMM, and CHARMM/OpenMM Simulations Using the CHARMM36 Additive Force Field. *J. Chem. Theory Comput.* **2016**, *12*, 405–413.
- (34) Klauda, J. B.; Venable, R. M.; Freites, J. A.; O'Connor, J. W.; Tobias, D. J.; Mondragon-Ramirez, C.; Vorobyov, I.; MacKerell, A. D.; Pastor, R. W. Update of the CHARMM All-Atom Additive Force Field for Lipids: Validation on Six Lipid Types. *J. Phys. Chem. B* **2010**, *114*, 7830–7843.
- (35) Huang, J.; Rauscher, S.; Nawrocki, G.; Ran, T.; Feig, M.; de Groot, B. L.; Grubmüller, H.; MacKerell, A. D. CHARMM36m: an improved force field for folded and intrinsically disordered proteins. *Nat. Methods* **2017**, *14*, 71–73.
- (36) Lay, W. K.; Miller, M. S.; Elcock, A. H. Reparameterization of Solute–Solute Interactions for Amino Acid–Sugar Systems Using Isopiestic Osmotic Pressure Molecular Dynamics Simulations. *J. Chem. Theory Comput.* **2017**, *13*, 1874–1882.
- (37) Kirschner, K. N.; Yongye, A. B.; Tschampel, S. M.; González-Outeiriño, J.; Daniels, C. R.; Foley, B. L.; Woods, R. J. GLYCAM06: A generalizable biomolecular force field. *Carbohydrates. J. Comput. Chem.* **2008**, *29*, 622–655.
- (38) Hess, B.; Kutzner, C.; Van Der Spoel, D.; Lindahl, E. GROMACS 4: Algorithms for highly efficient, load-balanced, and scalable molecular simulation. *J. Chem. Theory Comput.* **2008**, *4*, 435–447.
- (39) Pronk, S.; Páll, S.; Schulz, R.; Larsson, P.; Bjelkmar, P.; Apostolov, R.; Shirts, M. R.; Smith, J. C.; Kasson, P. M.; van der Spoel, D.; et al. GROMACS 4.5: a high-throughput and highly parallel open source molecular simulation toolkit. *Bioinformatics* **2013**, *29*, 845–854.
- (40) Páll, S.; Abraham, M. J.; Kutzner, C.; Hess, B.; Lindahl, E. Tackling Exascale Software Challenges in Molecular Dynamics Simulations with GROMACS. *Solving Softw. Challenges Exascale* **2015**, *8759*, 3–27.
- (41) Abraham, M. J.; Murtola, T.; Schulz, R.; Páll, S.; Smith, J. C.; Hess, B.; Lindahl, E. GROMACS: High performance molecular simulations through multi-level parallelism from laptops to supercomputers. *SoftwareX* **2015**, *1–2*, 19–25.
- (42) Berendsen, H. J. C.; Postma, J. P. M.; van Gunsteren, W. F.; DiNola, A.; Haak, J. R. Molecular dynamics with coupling to an external bath. *J. Chem. Phys.* **1984**, *81*, 3684–3690.
- (43) Parrinello, M.; Rahman, A. Polymorphic transitions in single crystals: A new molecular dynamics method. *J. Appl. Phys.* **1981**, *52*, 7182–7190.
- (44) Bussi, G.; Donadio, D.; Parrinello, M. Canonical sampling through velocity rescaling. *J. Chem. Phys.* **2007**, *126*, 014101.
- (45) Hess, B.; Bekker, H.; Berendsen, H. J. C.; Fraaije, J. G. E. M. LINCS: A linear constraint solver for molecular simulations. *J. Comput. Chem.* **1997**, *18*, 1463–1472.
- (46) Essmann, U.; Perera, L.; Berkowitz, M. L.; Darden, T.; Lee, H.; Pedersen, L. G. A smooth particle mesh Ewald method. *J. Chem. Phys.* **1995**, *103*, 8577–8593.
- (47) de Jong, D. H.; Singh, G.; Bennett, W. F. D.; Arnarez, C.; Wassenaar, T. A.; Schäfer, L. V.; Periole, X.; Tielemans, D. P.; Marrink, S. J. *Phys. Chem. B* **2021**, *125*, 5346–5357

- S. J. Improved Parameters for the Martini Coarse-Grained Protein Force Field. *J. Chem. Theory Comput.* **2013**, *9*, 687–697.
- (48) Yesylevskyy, S. O.; Schäfer, L. V.; Sengupta, D.; Marrink, S. J. Polarizable Water Model for the Coarse-Grained MARTINI Force Field. *PLoS Comput. Biol.* **2010**, *6*, No. e1000810.
- (49) Schmalhorst, P. S.; Deluweit, F.; Scherrers, R.; Heisenberg, C.-P.; Sikora, M. Overcoming the Limitations of the MARTINI Force Field in Simulations of Polysaccharides. *J. Chem. Theory Comput.* **2017**, *13*, 5039–5053.
- (50) López, C. A.; Rzepiela, A. J.; de Vries, A. H.; Dijkhuizen, L.; Hünenberger, P. H.; Marrink, S. J. Martini Coarse-Grained Force Field: Extension to Carbohydrates. *J. Chem. Theory Comput.* **2009**, *5*, 3195–3210.
- (51) Michalowsky, J.; Schäfer, L. V.; Holm, C.; Smiatek, J. A refined polarizable water model for the coarse-grained MARTINI force field with long-range electrostatic interactions. *J. Chem. Phys.* **2017**, *146*, 054501.
- (52) Hunt, C. J. Cryopreservation: Vitrification and Controlled Rate Cooling. In *Stem Cell Bank. Concepts Protoc.*; Crook, J. M., Ludwig, T. E., Eds.; Springer New York: New York, 2017; pp 41–77.
- (53) *The PyMOL Molecular Graphics System*, version 2.0; Schrödinger, LLC, 2020.
- (54) Andersen, H. D.; Wang, C.; Arleth, L.; Peters, G. H.; Westh, P. Reconciliation of opposing views on membrane–sugar interactions. *Proc. Natl. Acad. Sci. U. S. A.* **2011**, *108*, 1874–1878.
- (55) Yellin, N.; Levin, I. W. Hydrocarbon chain trans-gauche isomerization in phospholipid bilayer gel assemblies. *Biochemistry* **1977**, *16*, 642–647.
- (56) Leekumjorn, S.; Sum, A. K. Molecular studies of the gel to liquid-crystalline phase transition for fully hydrated DPPC and DPPE bilayers. *Biochim. Biophys. Acta, Biomembr.* **2007**, *1768*, 354–365.
- (57) Almeida, P. F. F.; Vaz, W. L. C.; Thompson, T. E. Lateral diffusion in the liquid phases of dimyristoylphosphatidylcholine/cholesterol lipid bilayers: a free volume analysis. *Biochemistry* **1992**, *31*, 6739–6747.
- (58) Miller, D. P.; de Pablo, J. J.; Corti, H. Thermophysical properties of trehalose and its concentrated aqueous solutions. *Pharm. Res.* **1997**, *14*, 578–90.